



# Detectable anthropogenic forcing on the long-term changes of summer precipitation over the Tibetan Plateau

Dan Zhao<sup>1,2</sup> · Lixia Zhang<sup>1,3</sup> · Tianjun Zhou<sup>1,2</sup>

Received: 6 August 2021 / Accepted: 2 February 2022 / Published online: 28 February 2022  
© The Author(s), under exclusive licence to Springer-Verlag GmbH Germany, part of Springer Nature 2022

## Abstract

Precipitation changes over the Tibetan Plateau (TP), “Asian Water Tower”, greatly affect water resources of the surrounding countries. A dipole pattern in summer precipitation trend over the TP is observed for 1961–2013, increasing over the north TP (NTP) and decreasing over the south TP (STP). Since the TP is one of the most vulnerable regions to climate change in the world, it is of great importance to investigate the role of anthropogenic forcing in the TP precipitation changes. Moisture budget analysis based on reanalysis reveals that the precipitation trends over NTP and STP are dominated by thermodynamic and dynamic terms of vertical moisture advection, respectively. Southward shift in the summer subtropical Asian westerly jet (AWJ) over the west of TP and northward shift in AWJ over the east of TP collaboratively result in the increase and decrease in dynamic component over NTP and STP, respectively. Here, we successfully detect the anthropogenic contribution to the NTP summer precipitation trends using the attribution experiments from the CLIVAR Climate of the 20th Century Plus Project (C20C+). The drying trends over STP are mainly controlled by internal variability, and the anthropogenic forcing is favorable for the drying trends. The impacts of anthropogenic forcing are twofold. First, human activity induced warming increases the specific humidity over TP, increasing the thermodynamic component of moisture budget. Second, the warming trend caused by anthropogenic forcing is unevenly distributed over the Eurasian continent, leading to the southward (northward) shift of AWJ over the west (east) of TP, favoring more precipitation over the NTP but less precipitation over the STP. This study provides evidence of the importance of anthropogenic forcing on the water cycle changes over the TP.

**Keywords** Tibetan Plateau · Precipitation · Attribution · Anthropogenic forcing · Westerly jet

## 1 Introduction

The Tibetan Plateau (TP), known as the “Asian Water Tower” and the “Third Pole”, is the highest plateau in the world and contains the largest number of glaciers outside the polar regions (Xu et al. 2008; Yao et al. 2012). As the head-water of many rivers in Asia, water cycle processes over the TP greatly affect the downstream hydrology and ecosystem

(Yao et al. 2012). TP can also modulate the Asian climate and global circulation through accelerating land-atmosphere heat exchange and changing the intensity and direction of circulation, due to its elevated topography (Immerzeel et al. 2010; Xu et al. 2014, 2015). TP is recognized as one of the most sensitive regions to climate changes, with the warming rate twice of global mean (Liu et al. 2021; Moore 2012). Significant changes in the ecosystems over the TP are reported in the past decades, including lake expansion and precipitation increase over the central TP (Lei et al. 2014; Zhang et al. 2019; Sun et al. 2020). However, the role of human activities in the climate change over TP and its mechanisms are still not fully understood. Given the importance of precipitation changes over the TP in the water cycle and water resources management of surrounding, it is of an urgent need to improve our knowledge about the impact of anthropogenic forcing on its precipitation changes (Gao et al. 2014; Gao et al. 2015a; Gao et al. 2015b; Sun et al. 2020; Liu et al. 2022).

✉ Lixia Zhang  
lixiazhang@mail.iap.ac.cn

<sup>1</sup> LASG, Institute of Atmospheric Physics, Chinese Academy of Sciences, Beijing 100029, China

<sup>2</sup> University of the Chinese Academy of Sciences, 100049 Beijing, China

<sup>3</sup> Collaborative Innovation Center on Forecast and Evaluation of Meteorological Disasters, Nanjing University of Information Science and Technology, Nanjing 210044, China

Many studies have reported the significant lake expansion in the central TP in recent decades (Zhang et al. 2017; Lei et al. 2014; Zhang et al. 2019), which is ascribed to the increased precipitation (Yang et al. 2011, 2018; Lei et al. 2014; Qiao et al. 2019) and melted glaciers induced by warming (Yao et al. 2012). The spring precipitation over the Sanjiangyuan region (31.5°–36.5°N, 89.5°–102.5°E) has increased at a rate of 0.05 mm day<sup>-1</sup> (10 year)<sup>-1</sup> for 1979–2009 and the summer precipitation shows interdecadal oscillation (Sun et al. 2018). The winter total precipitation over the eastern and central TP also shows significant increasing trends of 1.05 mm (10 year)<sup>-1</sup> for 1961–2007 in observation (You et al. 2012). The changes in annual mean TP precipitation exhibit spatial dependence. Increased precipitation in the central TP and decreased precipitation along the southern TP periphery are shown in gauge observation from 1984 to 2006 (Yang et al. 2011, 2014). Drying trends in the climatologically humid southeastern TP and wetting trends in the arid and semiarid northwestern TP are also found in gridded datasets during 1979–2011 (Gao et al. 2014). The Asian subtropical westerly jet (AWJ) and the South Asian monsoon are the dominant atmospheric circulations affecting the TP. The two centers of AWJ are located on the east and west of the TP, respectively (Du et al. 2016; Zhao et al. 2018). The northward shift and weakening of the AWJ near the TP are explored to be the mechanisms for the general wetting trend over the central TP (Gao et al. 2014; Sun et al. 2020; Liu et al. 2021). Li et al. (2021) recently also illustrated the phenomenon of inconsistent precipitation changes over the northern and southern TP, and interpreted the increased precipitation over the northern TP from the perspective of the activities of Tibetan Plateau vortices due to the strengthened AWJ there. However, it is not clear yet whether and how the human activities contribute to the observed dipole pattern of precipitation trend over TP in summer.

Detection and attribution analysis can quantify the relative contribution of anthropogenic and natural forcing to the changes in specific climate variables, which is helpful for formulating policies in handling climate change. Attribution studies on TP temperature show that anthropogenic greenhouse gases forcing dominate the TP warming (Chen et al. 2003; Duan et al. 2006; Zhou and Zhang 2021). Meanwhile, tree-ring series reveal the influence of anthropogenic forcing on the weakening annual temperature cycle over the TP (Duan et al. 2017). Because the observed regional precipitation changes are more difficult to capture than temperature in climate models, the attribution on regional precipitation changes is a great challenge (Gillett et al. 2004; Zhang et al. 2013). The results of attribution using optimal fingerprint method show that the increase in spring precipitation and low flow over the Sanjiangyuan region from 1979 to 2005 is controlled by anthropogenic forcing (Ji and Yuan 2019). In this study, we performed the detection and attribution

analysis on the summer (JJA) precipitation changes over the TP, since the precipitation over TP mainly falls in summer (Tong et al. 2014). The basic questions we address in this study are: (1) Does anthropogenic forcing contribute to the observed changes in TP summer precipitation? (2) If so, what are the physical mechanisms for the changes?

The remainder of this paper is organized as follows: We introduce the analysis methods and datasets used in this study in Sect. 2. Section 3 presents the main results including observed changes in summer TP precipitation, contribution of anthropogenic forcing to precipitation changes and the mechanisms behind it. Finally, the main results are summarized in Sect. 4.

## 2 Data and methods

### 2.1 Datasets

We use monthly precipitation for 1961–2013 on a 0.5° × 0.5° grid from two observation datasets, i.e., Climate Research Unit gridded Time Series (CRU TS) Version 4.0.3 (Harris et al. 2020) and Global Precipitation Climatology Centre (GPCC) Full Data Reanalysis Version 2018 (Schneider et al. 2018). The ensemble mean of the two precipitation is regarded as observation in this study. Previous studies have shown that these gridded precipitation datasets can reasonably represent the large-scale spatial and temporal characteristics of precipitation on the TP compared with rain gauge records, although they perform poorly in precisely portraying the topography-dependence of precipitation (Shi et al. 2017; Yang et al. 2018; Hamm et al. 2020). The circulation datasets are from the Japanese 55-year Reanalysis (JRA-55) dataset at a horizontal resolution of 1.25° × 1.25° for 1961–2013 (Kobayashi et al. 2015). The variables in JRA-55 used in this study include precipitation, evaporation, specific humidity, vertical velocity, horizontal winds, and geopotential height.

The model output used in this study are conducted by the Community Atmosphere Model version 5.1 (CAM5.1) from the Climate Variability and Predictability Research Program (CLIVAR) Climate of the Twentieth Century Plus (C20C+) Detection and Attribution Project (Folland et al. 2014; Angéilil et al. 2017). The model has two experiments, i.e., all forcing (CAM5-All) and natural forcing (CAM5-Nat), and each of them has 50 realizations. The CAM5-All is driven by observed external forcing, including observed sea surface temperature, greenhouse gases, tropospheric aerosols, volcanic aerosols and land cover, representing the real-world simulation. In CAM5-Nat, tropospheric aerosols, greenhouse gas, stratospheric ozone, and land cover are set to the estimated preindustrial level, and the anthropogenic contributions to sea surface temperature and sea ice coverage estimated from CMIP5 models using the optimal

fingerprinting method are subtracted from observations (Stone and Pall 2016; Stone et al. 2018). It represents the natural scenario unaffected by human activities. Therefore, the difference between the CAM5-All and CAM5-Nat shows the contribution of anthropogenic forcing. Details of the model driven data and setups are available in the above references and on the web site of the CLIVAR C20C+ Detection and Attribution Project (<http://portal.neresc.gov/c20c/main.html>). To verify the robustness of the results revealed by CAM5.1, we also analyzed the attribution outputs from the Hadley Centre Global Environmental Model version 3 (HadGEM3) from C20C+ as a reference, which only has 15 realizations in the all forcing (HadGEM-All) and natural forcing (HadGEM-Nat) experiment (Christidis et al. 2013). Mann-Kendall non-parametric test is used to examine the significance of linear trends.

### 2.2 Moisture budget analysis

A commonly used moisture budget analysis (Seager et al. 2010; Chou and Lan 2012) is performed in this study to investigate the physical mechanisms for the influence of human activities on summer TP precipitation changes, which is expressed as:

$$P' = E' - \partial_t \langle q \rangle - \langle V_h \cdot \nabla_h q \rangle' - \langle \omega \partial_p q \rangle' + \delta, \tag{1}$$

where  $P$ ,  $E$ ,  $q$ ,  $V_h$ , and  $\omega$  is precipitation, evaporation, specific humidity, horizontal winds, and vertical velocity, respectively.  $\langle \rangle$  denotes a column integration from surface to tropopause. Thus,  $-\langle V_h \cdot \nabla_h q \rangle'$  and  $-\langle \omega \partial_p q \rangle'$  represents the changes in horizontal and vertical moisture advection, respectively.  $\partial_t \langle q \rangle$  can be neglected on a seasonal scale.  $\delta$  is the residual term, which indicates the sub-seasonal transient eddy.

The changes in vertical moisture advection can be further divided as

$$-\langle \omega \partial_p q \rangle' = -\langle \bar{\omega} \partial_p \bar{q} \rangle' - \langle \omega' \partial_p \bar{q} \rangle' - \langle \omega \partial_p q' \rangle'. \tag{2}$$

The three terms on the right side of Eq. 2 denotes the thermodynamic (contribution of moisture changes), dynamic (contribution of atmospheric circulation changes) and non-linear component, respectively.

## 3 Results

### 3.1 Observed and simulated changes in summer TP precipitation

We first examine the performance of the CAM5.1 in simulating the climatological summer precipitation over the

TP (Fig. 1). The observed summer precipitation over the TP and surrounding region increases from northwest to southeast, with the maximum ( $\sim 1300 \text{ mm month}^{-1}$ ) on the southeastern edge of the TP (Fig. 1a, b). The reanalysis shows similar pattern with observation but with larger amount (Fig. 1c). The multi-model ensemble mean (MME) of CAM5-All can capture the distribution of the observed precipitation reasonably, but the precipitation amount in the model is larger than the observation over the whole TP, especially along the southern periphery (Fig. 1d). The pattern correlation coefficient between summer precipitation in CAM5-All MME and observation mean is 0.88 over the TP.

Then we show the distribution of precipitation trends derived from the observation and simulation in Fig. 2. Significant positive and negative trends of summer precipitation for 1961–2013 are displayed over the north and south TP in the observation, respectively (Fig. 2a). The positive trends are located in the climatologically arid northwestern part of TP, with the maximum trend reaching  $7.91 \text{ mm month}^{-1} \text{ decade}^{-1}$ . The negative trends are distributed along the climatologically humid southern edge of TP with a minimum of  $-18.25 \text{ mm month}^{-1} \text{ decade}^{-1}$ . The precipitation changes in JRA55 are similar to the observation, but with overestimated magnitudes (Fig. 2b). To detect the contribution of anthropogenic forcing to the precipitation changes, we show the spatial distribution of summer TP precipitation trends in CAM5-All and CAM5-Nat simulations in Fig. 2c, d. The CAM5-All MME can capture the dipole pattern exhibited in observation and JRA55 (Fig. 2c). More than 80% realizations of the CAM5-All show the same trend as the CAM5-All MME over the regions with significant trends, indicating the reliability of the precipitation trends derived from CAM5-All. In contrast to the observation and CAM5-All, the precipitation in CAM5-Nat MME decreases significantly over southwestern and northeastern TP, and increases over southeastern TP for 1961–2013 (Fig. 2d). As for the uncertainty of precipitation trends in the natural forcing only experiment, the ratio of realizations with the same sign as MME exceeds 80% over the southwestern TP regions with significant decreasing trends in MME. Thus, the decreasing trends over the south TP can be forced by internal variability. Based on the different distributions derived from CAM5-All and CAM5-Nat, it can be inferred that the observed dipole pattern of summer TP precipitation trends, particularly over the north TP, are markedly affected by anthropogenic forcing.

To quantify the contribution of anthropogenic forcing on precipitation changes, we selected two subregions based on precipitation trends in the observation to represent the north TP (NTP,  $32^\circ\text{--}40^\circ\text{N}$ ,  $70^\circ\text{--}98^\circ\text{E}$ ) and south TP (STP,  $25^\circ\text{--}31^\circ\text{N}$ ,  $75^\circ\text{--}105^\circ\text{E}$ ), respectively. The evolution of

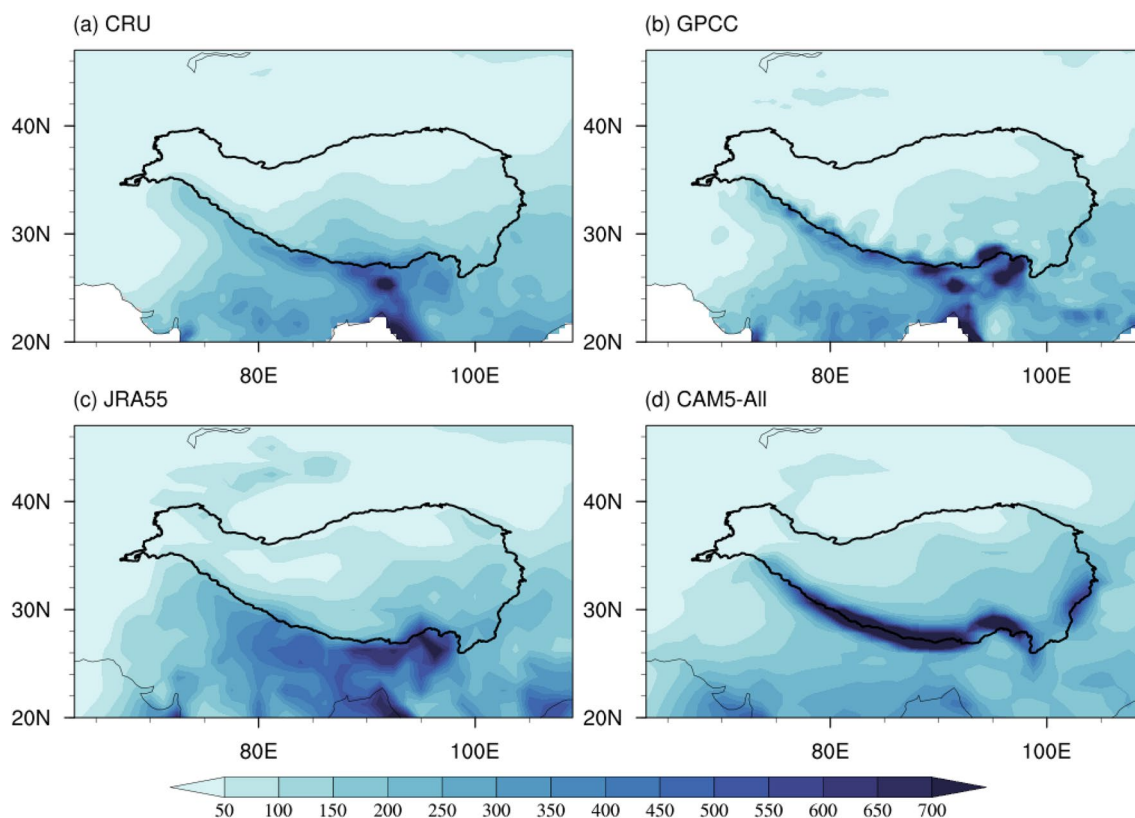


**Fig. 1** Spatial distribution of climatological summer precipitation ( $\text{mm month}^{-1}$ ) over the Tibetan Plateau for 1961–2013 in **a** CRU, **b** GPCC, **c** JRA55 and **d** CAM5-All MME

summer precipitation derived from the observation, reanalysis and model simulations averaged over NTP and STP are shown in Fig. 3a, b. As for observation, the regional mean summer precipitation in CRU (green line) and GPCC (yellow line) both show a positive trend over NTP, with an increasing rate at  $1.27 \text{ mm mon}^{-1} \text{ decade}^{-1}$  and  $1.31 \text{ mm mon}^{-1} \text{ decade}^{-1}$ , respectively (Fig. 3a). In contrast, the precipitation over STP decreased significantly by  $-3.32 \text{ mm mon}^{-1} \text{ decade}^{-1}$  and  $-2.55 \text{ mm mon}^{-1} \text{ decade}^{-1}$  in CRU and GPCC, respectively (Fig. 3b). The JRA55 can present the dipole precipitation trends.

The CAM5-All and CAM5-Nat experiments display different precipitation evolutions and trends. For the NTP, precipitation in CAM5-All MME shows increasing trend of  $1.70 \text{ mm mon}^{-1} \text{ decade}^{-1}$ , slightly higher than the observations, although the climate mean precipitation in CAM5-All is stronger than the observation. On the contrary, the CAM5-Nat MME simulates a decreasing trend of  $-1.01 \text{ mm mon}^{-1} \text{ decade}^{-1}$  (Fig. 3a). To assess the reliability of the attribution result, the probability density functions (PDF) of precipitation trends derived from 50 realizations of CAM5-All and CAM5-Nat simulations are compared (Fig. 3c). The observed NTP trend (green and yellow lines in Fig. 3c) can hardly happen in a natural forcing world (blue shading

in Fig. 3c), and only one out of the 50 realizations (2%) from CAM5-Nat shows comparable trend with the observation. The observed NTP precipitation trend falls outside the 5–95% confidence interval range ( $-2.86$  to  $0.85 \text{ mm mon}^{-1} \text{ decade}^{-1}$ ) in a natural forcing world. It indicates that the increasing NTP precipitation in the observation is hardly to happen without anthropogenic forcing. In contrast, the 5–95% confidence interval range of NTP trend in CAM5-All is  $0.40$ – $3.00 \text{ mm mon}^{-1} \text{ decade}^{-1}$  (red shading). The probability of NTP precipitation trend exceeding the observation is 76% in CAM5-All, which is 38 times of that in CAM5-Nat. Thus, the observed wetting trends of NTP can be attributed to the anthropogenic forcing. As for STP, both the CAM5-All MME and CAM5-Nat MME exhibit a decreasing trend (Fig. 3b). The decreasing trend in CAM5-All is more significant than that in CAM5-Nat. The observed precipitation trends are located within the 5–95% confidence interval range of both CAM5-All and CAM5-Nat. The probability of the decreasing precipitation trend exceeding the observation is 19.2% in the natural forcing world, while it increases to 59.1% under anthropogenic forcing, by a factor of 3 (Fig. 3d). Thus, the drying trends over STP are significantly controlled by internal variability, in accord with Yue et al. (2020), and the anthropogenic forcing is also favorable

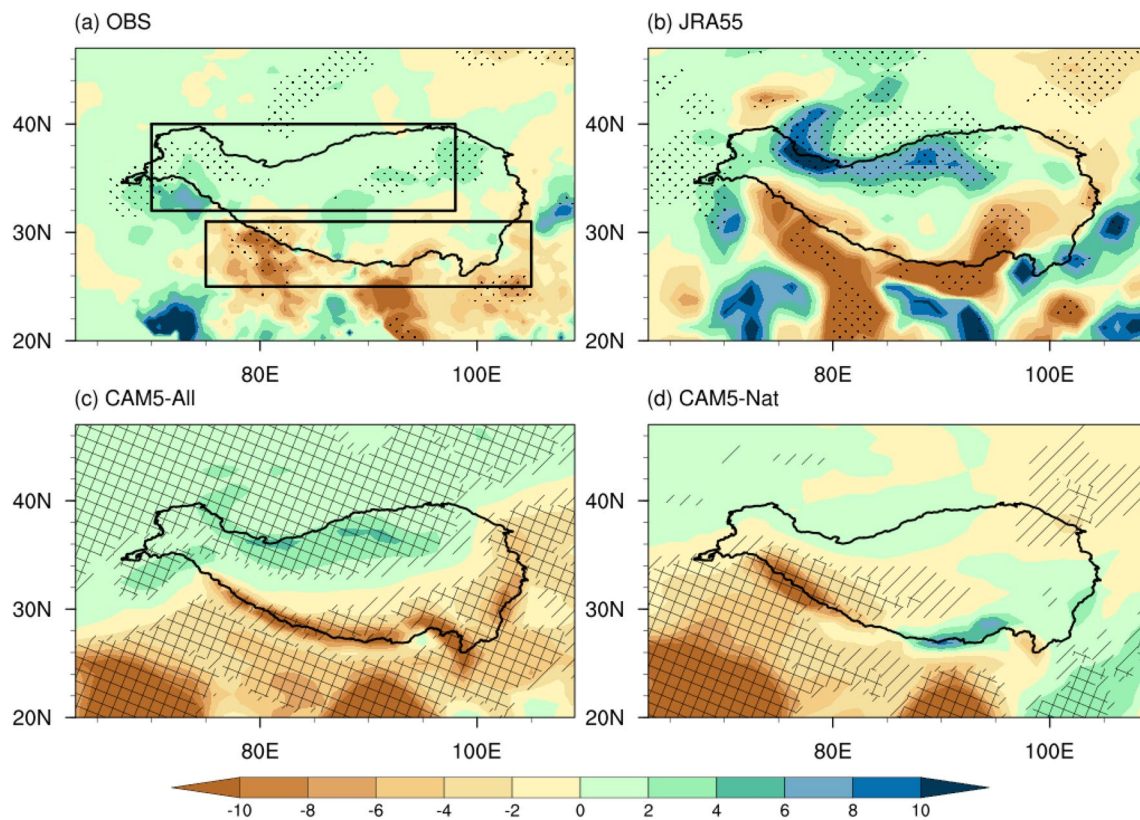


**Fig. 2** Summer precipitation trends ( $\text{mm month}^{-1} \text{decade}^{-1}$ ) over the Tibetan Plateau for 1961–2013 in **a** observations derived from the ensemble mean of CRU and GPCC; **b** JRA55; **c** CAM5-All MME; **d** CAM5-Nat MME. The black dots in **(a, b)** indicate that trends are statistically significant at the 5% level based on Mann-Kendall non-parametric test. Crossed lines in **(c, d)** indicate that trends are statis-

tically significant at the 5% level and more than 80% of 50 realizations agree on the sign of MME. Diagonal lines in **(c, d)** indicate that trends are statistically significant at the 5% level but fewer than 80% of 50 realizations agree on the sign of MME. The black curly line indicates the Tibetan Plateau. The black boxes in **(a)** indicate the NTP and STP in this study

for the drying trends. The Kolmogorov–Smirnov test shows that the precipitation trend PDF distributions from CAM5-All and CAM5-Nat are different over both NTP and STP (Fig. 3c, d), statistically significant at the 5% level. This further reveals that the impact of anthropogenic forcing on the TP precipitation trend is detectable.

### 3.2 Mechanisms for the influence of anthropogenic forcing on TP precipitation changes

To further investigate the physical mechanisms for the influence of human activities on summer TP precipitation changes, the moisture budget analysis is performed over the NTP and STP, respectively (Fig. 4). For the NTP, the increased precipitation is dominated by the increased vertical moisture advection term in JRA55. By further dividing it to dynamic and thermodynamic component, both of them contribute to the increased vertical moisture advection, and the thermodynamic term plays a dominant role (red bars in Fig. 4a). Over the STP, the decrease in precipitation is attributed to the diminishing vertical moisture advection, and it

is caused by less dynamic term due to suppressed ascent motion (red bars in Fig. 4b). The moisture budget in CAM5-All MME shows consistencies with JRA55, indicating that it can reproduce the physical mechanisms for precipitation changes over the TP reasonably. By contrast, the CAM5-Nat MME simulates opposite trends to JRA55 and CAM5-All for each dominant component mentioned above. For each dominant moisture budget process, the trend of JRA55 falls within the range of the CAM5-All realizations, while outside the range of the CAM5-Nat realizations, over both the NTP and STP. Clearly, anthropogenic forcing contributes to the wetting trend in NTP mainly by increasing the specific humidity, and to the drying trend in STP by suppressing the vertical motion, respectively. In addition, we also notice a large magnitude of residue term of the moisture budget over NTP, which is may due to imbalance of moisture budget in reanalysis caused by scare observation and complex topography over NTP.

The thermodynamic effect of anthropogenic forcing is relative clearly with global warming, since global warming can increase the atmospheric water holding capacity and

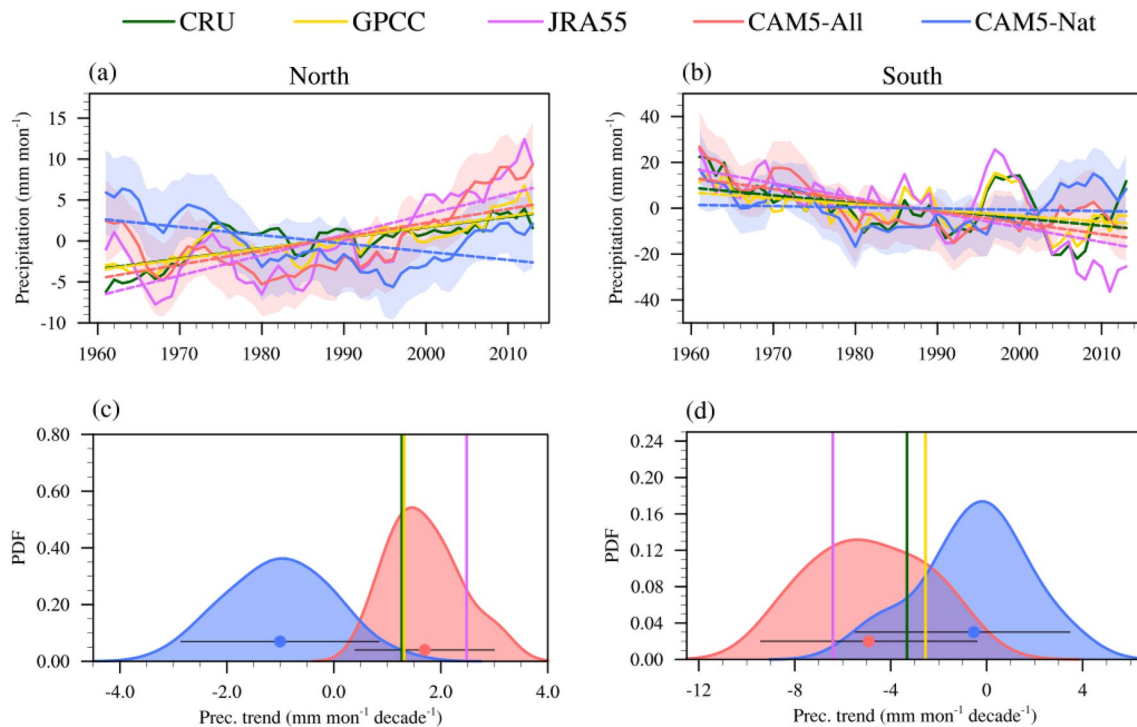


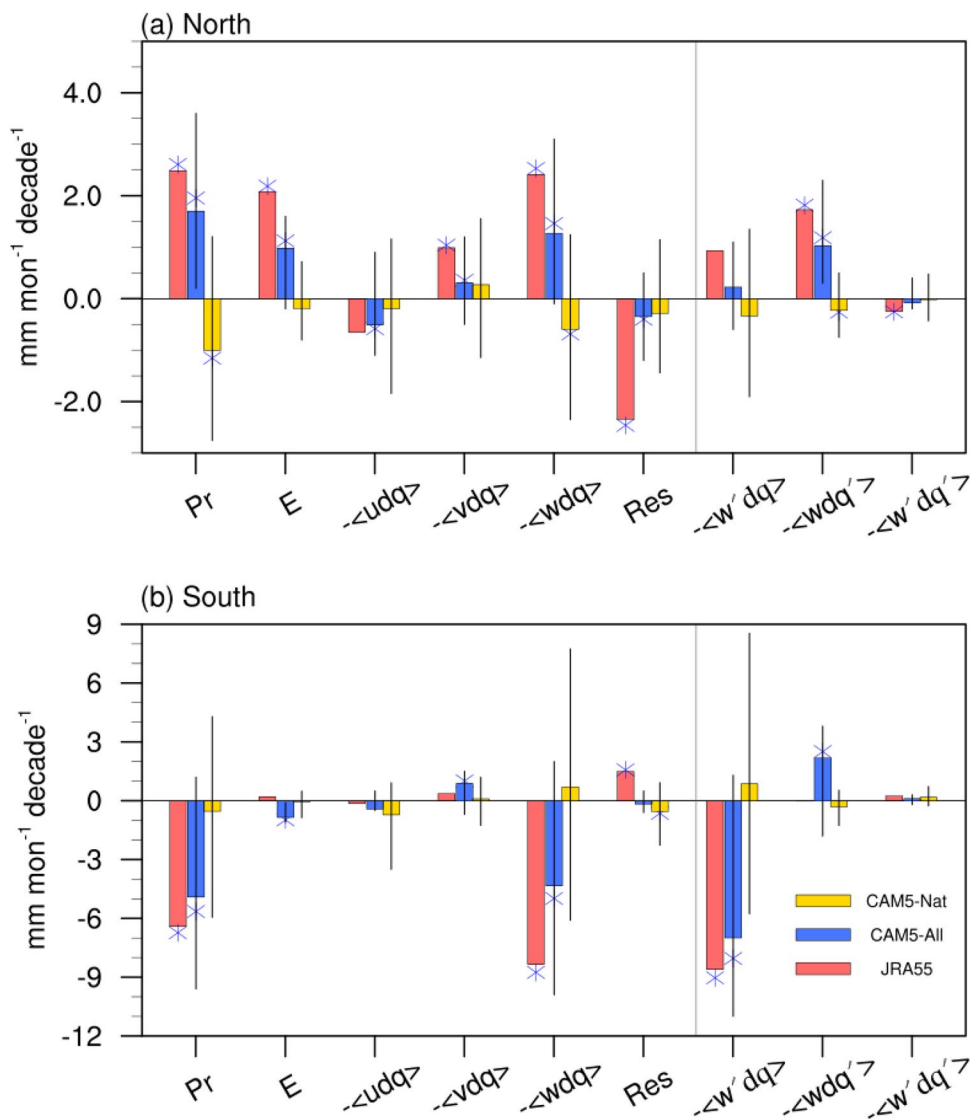
**Fig. 3** **a, b** The 5-year running mean summer precipitation anomalies ( $\text{mm month}^{-1}$ ) averaged over the **a** NTP and **b** STP for 1961–2013. CRU, GPCC, JRA55, CAM5-All ensemble mean and CAM5-Nat ensemble mean are indicated by the green, yellow, purple, red and blue lines, respectively. The red and blue shading denotes the standard deviation of the 50 realizations in CAM5-All and CAM5-Nat, respectively. The dashed lines are the linear trends. All trends are statistically significant at the 5% level except for the trend in CAM5-

Nat ensemble mean over STP; **c, d** The probability density functions of precipitation trends ( $\text{mm month}^{-1} \text{ decade}^{-1}$ ) over the **c** NTP and **d** STP from CAM5-All (red shading) and CAM5-Nat (blue shading). The green, yellow and purple lines denote the trends from CRU, GPCC and JRA55, respectively. The dots indicate ensemble mean of each experiment. The horizontal black lines indicate a range of 5–95% from the corresponding distribution. Significance test is based on the Mann–Kendall non-parametric test

then more moisture content. The distributions of summer precipitable water vapor trends over the TP derived from JRA55 and simulation MME are shown in Fig. 5. In JRA55, the precipitable water vapor over the central and north TP increases significantly, with positive trends increase from south to north. The largest trends are located on north periphery of the TP ( $> 5\% \text{ decade}^{-1}$ ), contributing to the wetting trend over NTP (Fig. 5a). The CAM5-All MME can reproduce the increasing trend and its meridional gradient, with maximum of 3–4%  $\text{decade}^{-1}$  over north TP (Fig. 5b). The CAM5-All show high consistency across the TP, with more than 80% of the realizations can capture the increasing trend of precipitable water vapor over the TP. By contrast, the precipitable water vapor in CAM5-Nat MME decreases over the TP, especially over west region (Fig. 5c). The increased atmospheric water vapor content over the NTP with anthropogenic forcing contributes to the increase in NTP precipitation. It is also worth noting that the increase in atmospheric water vapor content is partially attributed to the increase in precipitation, and precipitation trend can also contribute to local evaporation to alter local water vapor.

Previous studies have shown that the changes in summer precipitation over TP are modulated by the AWJ (Sun et al. 2020; Gao et al. 2014). Thus, we examined the first two EOF modes of 200-hPa zonal wind anomalies over Asia ( $25\text{--}55^\circ\text{N}$ ,  $40\text{--}140^\circ\text{E}$ ) and their correlation with the summer TP precipitation in the observation (Fig. 6). As reported in previous studies, the first mode represents the meridional movement of the AWJ axis with consistent east-west extension (Fig. 6c), and the second mode, a zonally asymmetric mode, reflects the inclination and rotation of the jet axis (Fig. 6d), with reverse meridional movement of jet's center over East and West Asia (Du et al. 2016; Li et al. 2020). We show the regression coefficient between the principal components (PC1 and PC2) corresponding to the first two EOF modes and summer TP precipitation, 500-hPa wind and integrated water vapor flux divergence in Fig. 6e–h, respectively. The increasing trend of PC1 (Fig. 6a) corresponds to the weakened and strengthened westerlies north and south of  $40^\circ\text{N}$ , respectively, accompany with air and water vapor convergence over east TP and divergence over southwest TP (Fig. 6e, g). Accordingly, the precipitation changes associated with EOF1 is below normal over the southwest TP, but

**Fig. 4** Trends ( $\text{mm month}^{-1} \text{decade}^{-1}$ ) for moisture budget components averaged over the **a** NTP and **b** STP. Pr is precipitation; E is evaporation;  $\langle -u dq \rangle$ ,  $\langle -v dq \rangle$ , and  $\langle -w dq \rangle$  are the zonal, meridional, and vertical moisture advection terms, respectively; Res is the residual term;  $\langle -w' dq' \rangle$ ,  $\langle -wdq' \rangle$ , and  $\langle -w' dq' \rangle$  are the dynamic, thermodynamic, and nonlinear components of vertical moisture advection term, respectively. The results from JRA-55, CAM5-All, and CAM5-Nat are denoted by red, blue, and yellow bars, respectively. Blue stars indicate that the trends are statistically significant at the 5% level by using the Mann–Kendall non-parametric test. The black lines indicate the range of the 50 realizations



above normal over the southeast TP (Fig. 6e). The regression coefficient between PC1 and observed precipitation is 0.05 and  $-1.43 \text{ mm mon}^{-1}$  averaged over the NTP and STP, respectively. For the second mode, positive trend of the PC2 (Fig. 6b) indicates that the jet stream is displaced southward for the center west of TP and northward near the TP, resulting in intensified and weakened westerlies over west and east of the TP, respectively. Such changes are also demonstrated in Sun et al. (2020). The large-scale circulation anomalies lead to anomalous air and water vapor flux convergence and divergence over NTP and STP, respectively (Fig. 6f, h). That is favorable for the increase and decrease in vertical moisture advection over NTP and STP, respectively. Hence, the precipitation regression pattern is similar to the linear trend for 1961–2013 (Fig. 6f), with wetter NTP and dryer STP (Fig. 6f). The regression coefficient between PC2 and precipitation is 1.06 and  $-2.22 \text{ mm mon}^{-1}$  averaged over the NTP and STP, respectively. The second mode of the AWJ

plays a dominant role in the dipole pattern of precipitation anomalies.

To detect the influence of human activities on the changes in the second mode of AWJ, we examined the evolutions and trends of the second mode of AWJ PC2 in CAM5-All and CAM5-Nat simulations (Fig. 7a). The PC2 in JRA55 and CAM5-All MME both show increase trend, but that in CAM5-Nat MME shows a significant decrease trend. The PDF of trends in PC2 derived from the 50 realizations of CAM5-All and CAM5-Nat are exhibited in Fig. 7b. The probability of the trend exceeding that in JRA55 increased from 2.0% in CAM5-Nat to 9.6% in CAM5-All, indicating that human activities have indispensable contribution to the increased trend in the second mode of AWJ, and then the dynamical term of TP precipitation trends as shown in Fig. 4.

To verify the robustness of the results in CAM5.1, we also analyzed the attribution outputs from the HadGEM3

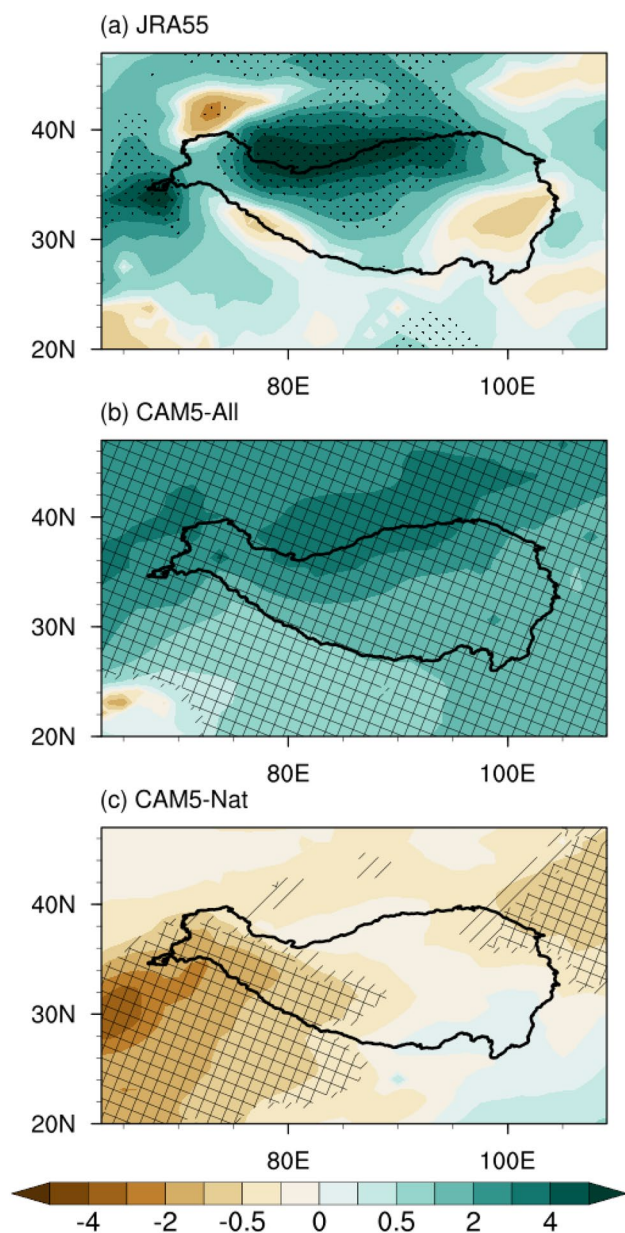


**Fig. 5** Summer precipitable water vapor trends ( $\% \text{ decade}^{-1}$ ) over the TP for 1961–2013 in **a** JRA55, **b** CAM5-All ensemble mean, **c** CAM5-Nat ensemble mean. Crossed lines in **b**, **c** indicate that trends are statistically significant at the 5% level and more than 80% of 50 realizations agree on the sign of MME. Diagonal lines in **c**, **d** indicate that trends are statistically significant at the 5% level but fewer than 80% of 50 realizations agree on the sign of MME. Significance test is based on the Mann–Kendall non-parametric test

with less realizations as a reference (Fig. 8). The dipole trends of TP summer precipitation also can be simulated by HadGEM-All (Fig. 8a), while the wetting trends over NTP are absent in HadGEM-Nat (Fig. 8b). Similar effects of the anthropogenic forcing to the precipitation changes over

NTP and STP are detected in the HadGEM3. Over NTP, the observed precipitation trends are located within the 5–95% confidence interval range of HadGEM3-All ( $-0.13$  to  $1.77 \text{ mm mon}^{-1} \text{ decade}^{-1}$ ), but fall outside the 5–95% of HadGEM3-Nat ( $-1.08$  to  $0.87 \text{ mm mon}^{-1} \text{ decade}^{-1}$ ). The probability of NTP precipitation trend exceeding the observation is also remarkably larger in HadGEM3-All than in HadGEM3-Nat (Fig. 8c). This demonstrates the robustness of the impact of anthropogenic forcing on NTP precipitation changes. The probability of the decreasing precipitation trend over STP exceeding the observation slightly increased in HadGEM3-All than in HadGEM3-Nat (Fig. 8d), highlighting the importance of internal variability, which is consistent with CAM5. As for the PC2 of AWJ, HadGEM-All MME shows increasing trend, consistent with JRA55, while the HadGEM-Nat MME simulates significant decreasing trend (Fig. 8e). The probability of the PC2 trend exceeding that in JRA55 also increased significantly with anthropogenic forcing in HadGEM3-All (Fig. 8f), in accord with the results from CAM5.1.

To clarify the cause of AWJ changes, Fig. 9 shows the trends of meridional 200-hPa geopotential height gradient during 1961–2013 in JRA55, CAM5-All MME and CAM5-Nat MME. To the west of the TP, the meridional geopotential height gradient increases south of  $40^\circ\text{N}$  but decreases north of it, resulting in the intensified ( $20^\circ\text{--}40^\circ\text{N}$ ,  $40^\circ\text{--}80^\circ\text{E}$ ) and weakened ( $40^\circ\text{--}55^\circ\text{N}$ ,  $40^\circ\text{--}80^\circ\text{E}$ ) westerly winds, respectively. Near the northeastern TP, the decreasing gradient weakens the westerly winds (Fig. 9a). Similar results are also reported in Li et al. (2021). This corresponds to the second mode of the westerly winds described above. The CAM5-All simulation shows similar pattern with JRA55, while the changes in NAT simulation are not significant (Fig. 9b, c). The CAM5-All realizations show high consistency. In the context of global warming, the tropospheric temperature increased in general, but the warming rate is unevenly distributed (Hong and Lu 2016; Peng et al. 2018). There is a cooling center over the west of the TP, which has been reported in several previous studies (Zhou and Zhang 2009; Zhao et al. 2014). It makes the distribution of changes in tropospheric temperature gradient around the TP uneven as shown in Fig. 9a. By comparing Fig. 9b, c, these changes are influenced by human activities significantly. Discrepancies between geopotential height gradient trends in the CAM5-All MME and JRA-55 are also seen (Fig. 9a, b). This is because CAM5-All MME is obtained by averaging 50 realizations, which reflects the overall impacts of all forcing and minimizes noise of internal variability. By examining results from each realization of CAM5-All, we can find some realizations highly consistent with that in the JRA55.



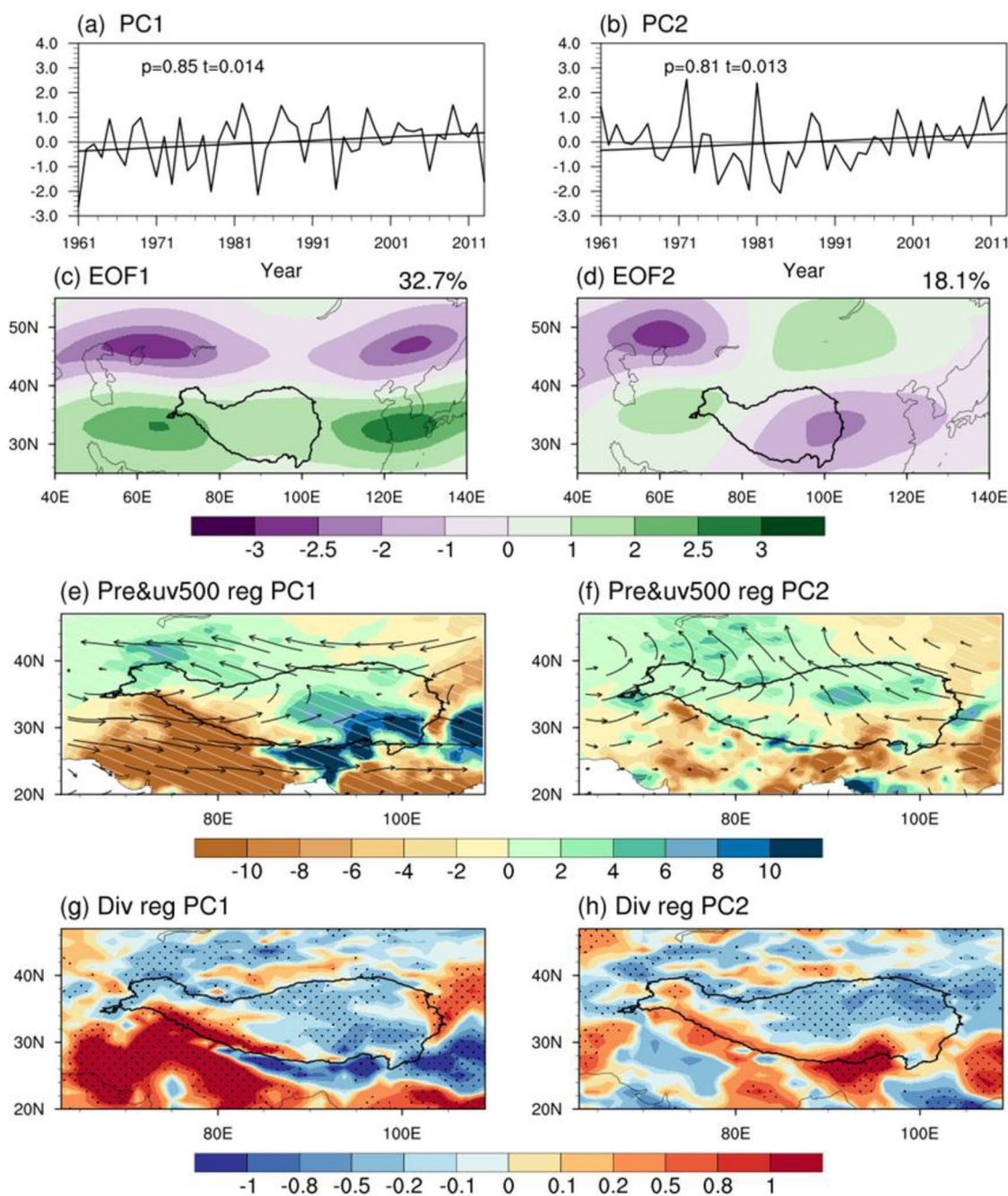


**Fig. 6** **a, b** Evolutions of principal components corresponding to the first two EOF modes in JRA55; **c, d** The first two EOF modes pattern ( $m s^{-1}$ ) for the summer 200-hPa zonal wind anomaly derived from JRA55; **e, f** Contour and vectors indicate the regression coefficients between principal components and summer precipitation in observa-

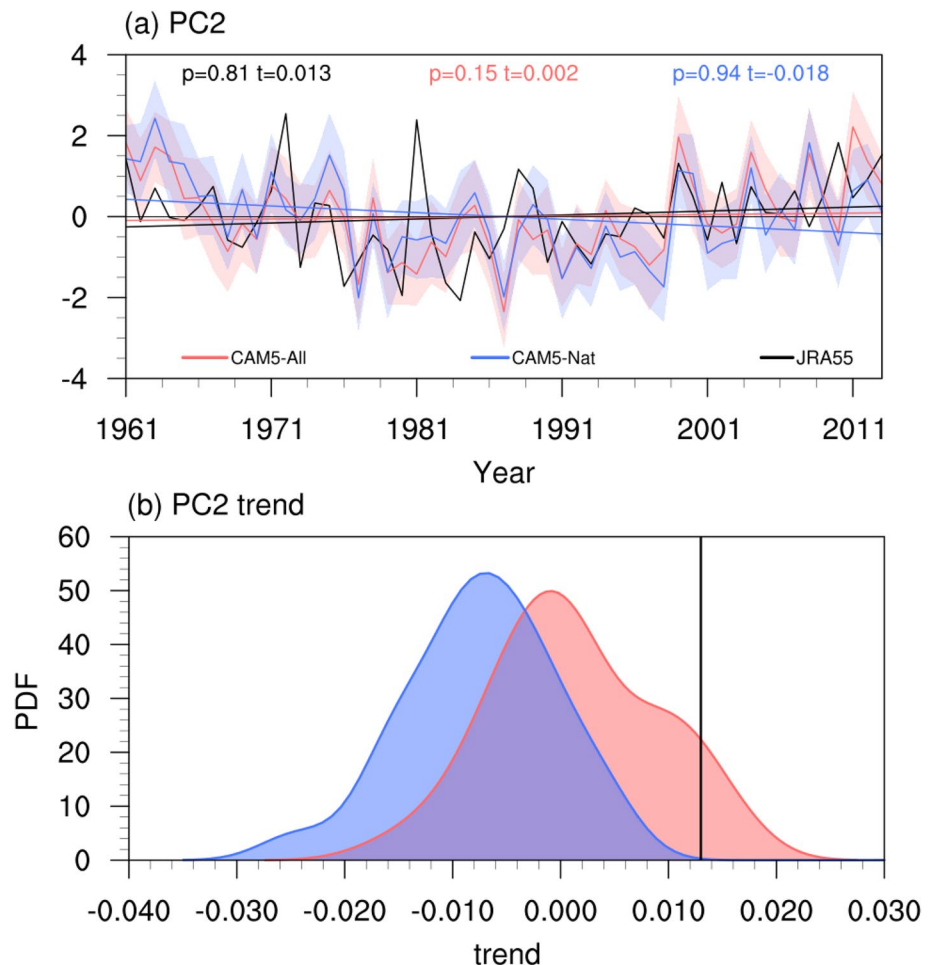
tion ( $mm month^{-1}$ ), 500-hPa wind in JRA55 ( $m s^{-1}$ , only the vectors statistically significant at the 5% level are shown), respectively; **g, h** The regression coefficients between the principal components of the first two leading modes and the summer integrated water vapor flux divergence ( $10^{-5} kg m^{-2} s^{-1}$ )

### 4 Summary

The Tibetan Plateau is the headwater of many rivers in Asia, and the precipitation changes over the TP greatly affect the downstream hydrology and ecosystem. Since the TP is

one of the most sensitive regions to climate change, it is of great importance to investigate the role of anthropogenic forcing on the TP precipitation changes. In this study, the anthropogenic contribution to the summer TP precipitation changes from 1961 to 2013 is detected using outputs from

**Fig. 7 a** Evolutions of PC2 in JRA55 (black line), CAM5-All ensemble mean (red line) and CAM5-Nat ensemble mean (blue line). The red and blue shading denote the standard deviation of the 50 realizations in CAM5-All and CAM5-Nat, respectively. The straight lines indicate corresponding linear trends. The  $p$  denotes probability and  $t$  denotes trend by using the Mann–Kendall non-parametric test; **b** The probability density functions of PC2 trends ( $\text{year}^{-1}$ ) from CAM5-All (red line) and CAM5-Nat (blue line). The black line denotes the trend from JRA55



the Climate Variability and Predictability Research Program (CLIVAR) Climate of the Twentieth Century Plus (C20C+) Detection and Attribution Project. The mechanisms for the impact of anthropogenic forcing are also examined. The main findings are summarized below:

1. Increased precipitation and decreased precipitation for 1961–2013 is exhibited over the north TP and southern TP periphery, respectively. The positive trends with the maximum rate at  $7.91 \text{ mm month}^{-1} \text{ decade}^{-1}$  lies in the northwestern corner of TP. The negative trends are distributed along the southern periphery with the minimum of  $-18.25 \text{ mm month}^{-1} \text{ decade}^{-1}$ .
2. The role of anthropogenic forcing on the observed trends in summer TP precipitation is successfully detected. The probability of NTP precipitation trend in the all forcing experiment of CAM5.1 (CAM5-All) with the magnitude exceeding the observation is 76%, significantly different from 2% in the natural only forcing experiment (CAM5-Nat). The drying trends over STP are mainly controlled by internal variability, and the anthropogenic forcing is favorable for the drying trends. The probability of the

declined STP precipitation trend exceeding the observation is 19.2% in CAM5-Nat, while it increases to 59.1% under anthropogenic forcing, by a factor of 3.

3. Anthropogenic forcing contributes to the wetting trend in NTP mainly by increasing specific humidity, and to the drying trend in STP by suppressing the vertical motion through shifting the AWJ southward, respectively. The thermodynamic term of anthropogenic forcing is manifested as increased atmospheric moisture content induced by global warming. Because warming trend in troposphere caused by human activities are spatially unevenly distributed, the mid-latitude jet stream shifted southward and northward for the center west of and near the TP, respectively, with intensified and weakened westerlies over west and east of the TP. It led to anomalous water vapor convergence and divergence over NTP and STP, respectively, favorable for the increase and decrease in the vertical motion over NTP and STP.

The rapid global warming in the past decades has brought remarkable changes to the water cycle over the Tibetan Plateau. The role of anthropogenic forcing in surface warming

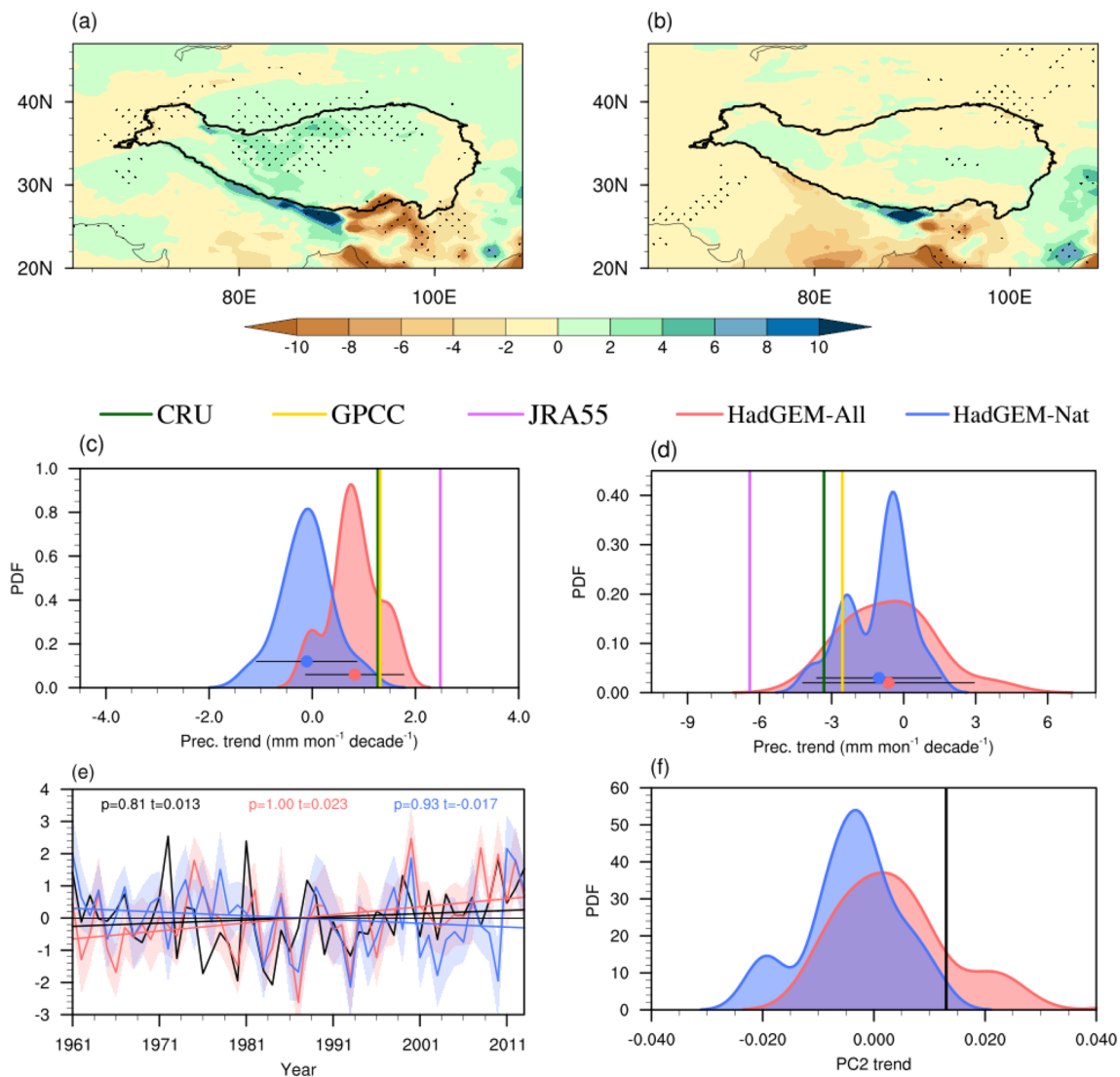


**Fig. 8** **a, b** Summer precipitation trends (mm month<sup>-1</sup> decade<sup>-1</sup>) over the Tibetan Plateau for 1961–2013 in **a** HadGEM-All and **b** HadGEM-Nat; **c, d** The probability density functions of precipitation trends (mm month<sup>-1</sup> decade<sup>-1</sup>) over the **c** NTP and **d** STP from HadGEM-All (red line) and HadGEM-Nat (blue line). The green, yellow and purple lines denote the trends from CRU, GPCC and JRA55, respectively. The dots indicate ensemble mean. The horizontal black lines indicate a range of 5–95% from the corresponding distribution;

**e** Evolutions of PC2 in JRA55 (black line), HadGEM-All ensemble mean (red line) and HadGEM-Nat ensemble mean (blue line). The red and blue shading denote the standard deviation of the 15 realizations in HadGEM-All and HadGEM-Nat, respectively; **f** The probability density functions of PC2 trends from HadGEM-All (red line) and HadGEM-Nat (blue line). The black line denotes the trend from JRA55. Significance test is based on the Mann-Kendall non-parametric test

has been well detected and attributed, implying a high risk in the glacier retreat, and degradation of permafrost due to surface warming (Zhou and Zhang 2021; Yao et al. 2019). In comparison, the understanding on the role of human influence in large-scale circulation and precipitation trends is relatively unclear so far. This study suggests that the dipole pattern of summer precipitation trend over the TP in the past sixty years are greatly affected by human influence due to the increase of moisture holding capacity and large-scale circulation change under human-induced global warming. It provides scientific evidence for the inhomogeneous

shrinkage of glacier across the TP, i.e. negative mass balance over the Himalayas (South TP) but less change in the eastern Pamir (Northwest TP) due to anthropogenic forcing (Yao et al. 2012, 2019). If the decadal internal variability controlling the current STP drying continue under further global warming, an accelerated glacier collapsing over the STP would be expected, which would greatly threaten water supplies and increase geohazard events over the surrounding regions. Thus, adaptation and mitigation measures should be taken to avoid potential environmental challenges caused by climate change in the near future.

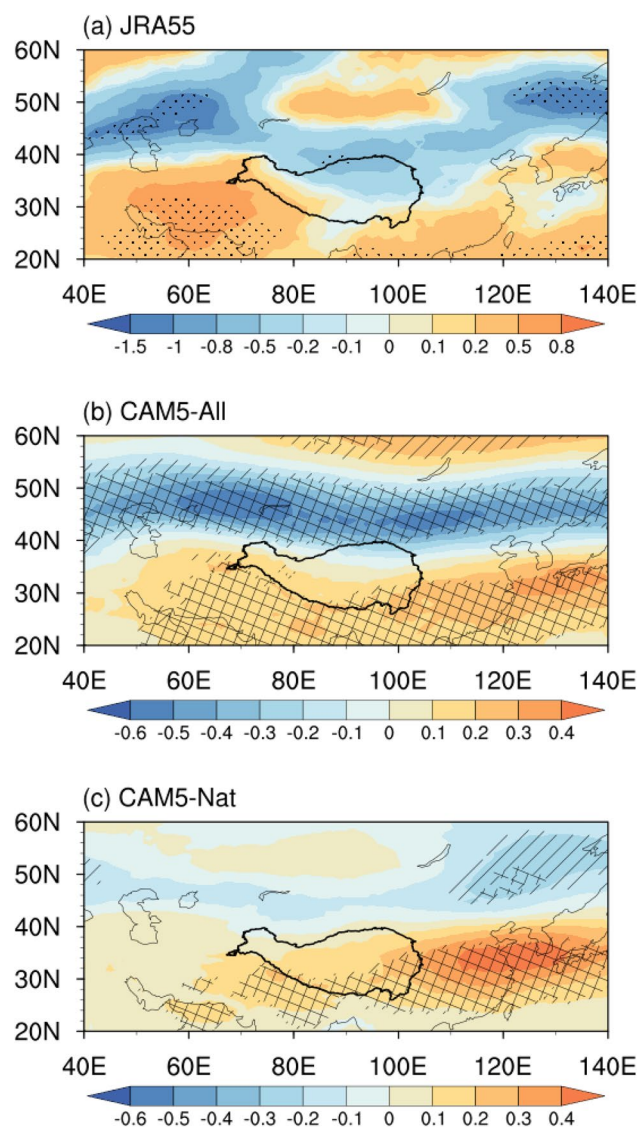


**Fig. 9** Summer 200-hPa geopotential height gradient trends ( $\text{gpm decade}^{-1}$ ) for 1961–2013 in **a** JRA55; **b** CAM5-All ensemble mean; **c** CAM5-Nat ensemble mean. Crossed lines in **b**, **c** indicate that trends are statistically significant at the 5% level and more than 80% of 50 realizations agree on the sign of MME. Diagonal lines in **b**, **c** indicate that trends are statistically significant at the 5% level but fewer than 80% of 50 realizations agree on the sign of MME. Significance test is based on the Mann–Kendall non-parametric test

**Acknowledgements** This work is supported by Strategic Priority Research Program of the Chinese Academy of Sciences (Grant No. XDA20060102) and the Second Tibetan Plateau Scientific Expedition and Research (STEP) program (Grant No. 2019QZKK0102).

**Funding** Strategic Priority Research Program of the Chinese Academy of Sciences (Grant No. XDA20060102) and the Second Tibetan Plateau Scientific Expedition and Research (STEP) program (Grant No. 2019QZKK0102).

**Availability of data and material** All original data that support the findings of this study are openly available at <http://search.diasjp.net/en/dataset/JRA55>, <http://portal.nersc.gov/c20c/data.html>, <https://catalogue.ceda.ac.uk/uuid/edf8febfdaad48abb2cbaf7d7e846a86>, [ftp://ftp.dwd.de/pub/data/gpcc/html/fulldata\\_v7\\_doi\\_download.html](ftp://ftp.dwd.de/pub/data/gpcc/html/fulldata_v7_doi_download.html).

## Declarations

**Conflict of interest** The authors declare no competing interests.

## References

- Angéil O, Stone D, Wehner M, Paciorek C, Krishnan H, Collins W (2017) An independent assessment of anthropogenic attribution statements for recent extreme temperature and rainfall events. *J Clim* 30:5–16. <https://doi.org/10.1175/JCLI-D-16-0077.1>
- Chen B, Chao W, Liu X (2003) Enhanced climatic warming in the Tibetan Plateau due to doubling CO<sub>2</sub>: a model study. *Clim Dyn* 20:401–413. <https://doi.org/10.1007/s00382-002-0282-4>
- Chou C, Lan CW (2012) Changes in the annual range of precipitation under global warming. *J Clim* 25:222–235. <https://doi.org/10.1175/JCLI-D-11-00097.1>
- Christidis N et al (2013) A new HadGEM3-A-based system for attribution of weather- and climate-related extreme events. *J Clim* 26:2756–2783. <https://doi.org/10.1175/JCLI-D-12-00169.1>
- Du Y, Li T, Xie Z, Zhu Z (2016) Interannual variability of the Asian subtropical westerly jet in boreal summer and associated with circulation and SST anomalies. *Clim Dyn* 46:2673–2688. <https://doi.org/10.1007/s00382-015-2723-x>
- Duan A et al (2006) New proofs of the recent climate warming over the Tibetan Plateau as a result of the increasing greenhouse gases emissions. *Chin Sci Bull* 51:1396–1400. <https://doi.org/10.1007/s11434-006-1396-6>
- Duan J et al (2017) Weakening of annual temperature cycle over the Tibetan Plateau since the 1870s. *Nat Commun* 8:1–7. <https://doi.org/10.1038/ncomms14008>
- Folland C, Stone D, Frederiksen C, Karoly D, Kinter J (2014) The International CLIVAR Climate of the 20th Century Plus (C20C+) project: report of the sixth workshop. *CLIVAR Exch* 19:57–59
- Gao Y, Cuo L, Zhang Y et al (2014) Changes in moisture flux over the Tibetan plateau during 1979–2011 and possible mechanisms. *J Clim* 27:1876–1893. <https://doi.org/10.1175/JCLI-D-13-00321.1>
- Gao Y, Leung L, Zhang Y et al (2015) Changes in moisture flux over the Tibetan Plateau during 1979–2011: insights from a high-resolution simulation. *J Clim* 28:4185–4197. <https://doi.org/10.1175/JCLI-D-14-00581.1>
- Gao Y, Li X, Leung L et al (2015b) Aridity changes in the Tibetan Plateau in a warming climate. *Environ Res Lett* 10:034013. <https://doi.org/10.1088/1748-9326/10/3/034013>
- Gillett N, Weaver A, Zwiers F, Wehner M (2004) Detection of volcanic influence on global precipitation. *Geophys Res Lett* 31:L12217. <https://doi.org/10.1029/2004GL020044>
- Hamm A et al (2020) Intercomparison of gridded precipitation datasets over a sub-region of the Central Himalaya and the Southwestern Tibetan Plateau. *Water* 12(11):3271. <https://doi.org/10.3390/w12113271>
- Harris I, Osborn T, Jones P, Lister D (2020) Version 4 of the CRU TS monthly high-resolution gridded multivariate climate dataset. *Sci Data* 7:1–18. <https://doi.org/10.1038/s41597-020-0453-3>
- Hong X, Lu R (2016) The meridional displacement of the summer Asian jet, Silk Road Pattern, and tropical SST anomalies. *J Clim* 29:3753–3766. <https://doi.org/10.1175/JCLI-D-15-0541.1>

- Immerzeel W, Van Beek L, Bierkens M (2010) Climate change will affect the Asian water towers. *Science* 328:1382–1385. <https://doi.org/10.1126/science.1183188>
- Ji P, Yuan X (2019) High resolution land surface modeling of hydrological changes over the Sanjiangyuan region in the eastern Tibetan Plateau: 2. Impact of climate and land cover change. *J Adv Model Earth Sy* 10:2829–2843. <https://doi.org/10.1029/2018MS001413>
- Kobayashi S et al (2015) The JRA-55 reanalysis: general specifications and basic characteristics. *J Meteorol Soc Japan* 93:5–48. <https://doi.org/10.2151/jmsj.2015-001>
- Lei Y, Yang K, Wang B et al (2014) Response of inland lake dynamics over the Tibetan Plateau to climate change. *Clim Change* 125:281–290. <https://doi.org/10.1007/s10584-014-1175-3>
- Li D, Chen H, Liu P, Zhou C (2020) Zonally asymmetric mode of anomalous activity in summer Asian subtropical westerly jet and its possible sources. *Theor Appl Climatol* 139:17–32. <https://doi.org/10.1007/s00704-019-02934-5>
- Li L, Zhang R, Wen M, Lv J (2021) Regionally different precipitation trends over the Tibetan Plateau in the warming context: a perspective of the Tibetan Plateau vortices. *Geophys Res Lett* 48(11):e2020GL091680. <https://doi.org/10.1029/2020GL091680>
- Liu Y, Chen H, Hu X (2021) The unstable relationship between the precipitation dipole pattern in the Tibetan Plateau and summer NAO. *Geophys Res Lett* 48(4):e2020GL091941. <https://doi.org/10.1029/2020GL091941>
- Liu Z, Gao Y, Zhang G (2022) How well can a convection-permitting-modelling improve the simulation of summer precipitation diurnal cycle over the Tibetan Plateau? *Clim Dyn*. <https://doi.org/10.1007/s00382-021-06090-3>
- Ma S, Zhou T, Stone D, Polson D et al (2017) Detectable anthropogenic shift toward heavy precipitation over Eastern China. *J Clim* 30:1381–1396. <https://doi.org/10.1175/JCLI-D-16-0311.1>
- Moore G (2012) Surface pressure record of Tibetan Plateau warming since the 1870s. *Q J R Meteorol Soc* 138:1999–2008. <https://doi.org/10.1002/qj.1948>
- Peng et al (2018) Human contribution to the increasing summer precipitation in central Asia from 1961 to 2013. *J Clim* 31:8005–8021. <https://doi.org/10.1175/JCLI-D-17-0843.1>
- Qiao B, Zhu L, Yang R (2019) Temporal-spatial differences in lake water storage changes and their links to climate change throughout the Tibetan Plateau. *Remote Sens Environ* 222:232–243. <https://doi.org/10.1016/j.rse.2018.12.037>
- Schneider U, Becker A, Finger P, Meyer-Christoffer A, Ziese M (2018) Precipitation from rain-gauges built on GTS-based and historical data. Global Precipitation Climatology Centre, GPCP Full Data Monthly Product Version 2018 at 0.5°: Monthly Land-Surface
- Seager R, Naik N, Vecchi GA (2010) Thermodynamic and dynamic mechanisms for large-scale changes in the hydrological cycle in response to global warming. *J Clim* 23:4651–4668. <https://doi.org/10.1175/2010JCLI3655.1>
- Shi H, Li T, Wei J (2017) Evaluation of the gridded CRU TS precipitation dataset with the point rain gauge records over the Three-River Headwaters Region. *J Hydrol* 548:322–332. <https://doi.org/10.1016/j.jhydrol.2017.03.017>
- Stone DA, Pall P (2016) A benchmark estimate of the effect of anthropogenic emissions on the ocean surface. *J Adv Model Earth Syst*. <http://portal.nersc.gov/c20c/pub.html>
- Stone DA, Risser MD, Angéil OM et al (2018) A basis set for exploration of sensitivity to prescribed ocean conditions for estimating human contributions to extreme weather in CAM5. 1-1degree. *Weather Climate Extremes* 19:10–19. <https://doi.org/10.1016/j.wace.2017.12.003>
- Sun B, Wang H (2018) Interannual variation of the spring and summer precipitation over the three river source region in china and the associated regimes. *J Clim* 31:7441–7457. <https://doi.org/10.1175/JCLI-D-17-0680.1>
- Sun J, Yang K, Guo W et al (2020) Why has the inner Tibetan Plateau become wetter since the mid-1990s? *J Clim* 33:8507–8522. <https://doi.org/10.1175/JCLI-D-19-0471.1>
- Tong K, Su F, Yang D et al (2019) Tibetan Plateau precipitation as depicted by gauge observations, reanalyses and satellite retrievals. *Int J Climatol* 34:265–285. <https://doi.org/10.1002/joc.3682>
- Wu G, Duan A, Liu Y et al (2015) Tibetan Plateau climate dynamics: recent research progress and outlook. *Natl Sci Rev* 2:100–116. <https://doi.org/10.1093/nsr/nwu045>
- Xu X, Lu C, Shi X, Gao S (2008) World water tower: an atmospheric perspective. *Geophys Res Lett* 35:L20815. <https://doi.org/10.1029/2008GL035867>
- Xu X, Zhao T, Lu C et al (2014) An important mechanism sustaining the atmospheric “water tower” over the Tibetan Plateau. *Atmos Chem Phys* 14:11287–11295. <https://doi.org/10.5194/acp-14-11287-2014>
- Yang K, Ye B, Zhou D et al (2011) Response of hydrological cycle to recent climate changes in the Tibetan Plateau. *Clim Change* 109:517–534. <https://doi.org/10.1007/s10584-011-0099-4>
- Yang K, Wu H, Qin J et al (2014) Recent climate changes over the Tibetan Plateau and their impacts on energy and water cycle: a review. *Glob Planet Change* 112:79–91. <https://doi.org/10.1016/j.gloplacha.2013.12.001>
- Yang K, Lu H, Yue S et al (2018) Quantifying recent precipitation change and predicting lake expansion in the Inner Tibetan Plateau. *Clim Change* 147:149–163. <https://doi.org/10.1007/s10584-017-2127-5>
- Yao T, Thompson L, Yang W et al (2012) Different glacier status with atmospheric circulations in Tibetan Plateau and surroundings. *Nat Clim Change* 2:663–667. <https://doi.org/10.1038/nclimate1580>
- Yao T, Xue Y, Chen D, Chen F et al (2019) Recent third pole’s rapid warming accompanies cryospheric melt and water cycle intensification and interactions between monsoon and environment: multi-disciplinary approach with observations, modeling, and analysis. *Bull Am Meteorol Soc* 100(3):423–444
- You Q, Fraedrich K, Ren G et al (2012) Inconsistencies of precipitation in the eastern and central Tibetan Plateau between surface adjusted data and reanalysis. *Theor Appl Climatol* 109:485–496. <https://doi.org/10.1007/s00704-012-0594-1>
- Yue S et al (2020) Mechanisms of the decadal variability of monsoon rainfall in the southern Tibetan Plateau. *Environ Res Lett* 16:014011. <https://doi.org/10.1088/1748-9326/abc36>
- Zhang X, Wan H, Zwiers F, Hegerl G, Min S (2013) Attributing intensification of precipitation extremes to human influence. *Geophys Res Lett* 40:5252–5257. <https://doi.org/10.1002/grl.51010>
- Zhang G, Yao T, Piao S et al (2017) Extensive and drastically different alpine lake changes on Asia’s high plateaus during the past four decades. *Geophys Res Lett* 44:252–260. <https://doi.org/10.1002/2016GL072033>
- Zhang G, Yao T, Chen W et al (2019) Regional differences of lake evolution across China during 1960s–2015 and its natural and anthropogenic causes. *Remote Sens Environ* 221:386–404. <https://doi.org/10.1016/j.rse.2018.11.038>
- Zhao Y et al (2014) Impact of the middle and upper tropospheric cooling over Central Asia on the summer rainfall in the Tarim basin, China. *J Clim* 27:4721–4732. <https://doi.org/10.1175/JCLI-D-13-00456.1>
- Zhao Y et al (2018) Evaluation of the subtropical westerly jet and its effects on the projected summer rainfall over central asia using multi-cmip5 models. *Int J Climatol* 38:1176–1189. <https://doi.org/10.1002/joc.5443>
- Zhou T, Zhang J (2009) Harmonious inter-decadal changes of July–August upper tropospheric temperature across the North Atlantic, Eurasian continent, and North Pacific. *Adv Atmos Sci* 26:656–665. <https://doi.org/10.1007/s00376-009-9020-8>

- Zhou T, Zhang W (2021) Anthropogenic warming of Tibetan Plateau and constrained future projection. *Environ Res Lett* 16:044039. <https://doi.org/10.1088/1748-9326/abede8>
- Zhou T, Zhang W (2021) Anthropogenic warming of Tibetan Plateau and constrained future projection. *Environ Res Lett* 16:044039. <https://doi.org/10.1088/1748-9326/abede8>

**Publisher's Note** Springer Nature remains neutral with regard to jurisdictional claims in published maps and institutional affiliations.